Main Manuscript for

An opened pre-40S platform enables temporal regulation of Fap7.

Jay Rai[1,2], Melissa D. Parker[2,3], Haina Huang[3], Stefan Choy[3], Homa Ghalei[3,4], Matthew C. Johnson[1,5], Katrin Karbstein[3,6*] and M. Elizabeth Stroupe[1*]

[1] Department of Biological Science and the Institute of Molecular Biophysics, Florida State University, Tallahassee, Florida, 32306
[2] These authors contributed equally
[3] Department of Integrative Structural and Computational Biology, The Scripps Research Institute, Jupiter, Florida, 33458
[4] Present address: Emory University School of Medicine, Department of Biochemistry, Atlanta, Georgia
[5] Present address: University of Washington, Department of Biochemistry, 1959 NE Pacific Street, Box 357350, Seattle, WA 98195
[6] HHMI Faculty Scholar
* To whom correspondence should be addressed: Katrin Karbstein and M. Elizabeth Stroupe

Email: kkarbst@scripps.edu; mestroupe@bio.fsu.edu

ORCIDs: Stroupe: 0000-0002-4393-1951

Karbstein: 0000-0002-4034-1331

Classification

Biological Sciences, Biophysics and Computational Biology

Keywords

Ribosome assembly, small ribosome subunit, cryo-EM

Author Contributions

J.R. and H.G. prepared samples; J.R. and M.E.S. carried out structure reconstruction; M.D.P., H.H., H.G. and S.C. carried out yeast analyses; M.C.J. performed cryo-EM analysis of pre-40S; K.K. and M.E.S. conceived of the experiments and wrote the paper.

This PDF file includes:

Main Text
Figs. 1 to 4

Abstract

During their maturation, nascent 40S subunits enter a translation-like quality control cycle, where they are joined by mature 60S subunits to form 80S-like ribosomes. While these assembly intermediates are essential for maturation and quality control, how they form, and how their structure promotes quality control remains unknown. To address these questions, we determined the structure of an 80S-like ribosome assembly intermediate to an overall resolution of 3.4 Å. The structure, validated by biochemical data, resolves a large body of previously paradoxical data and illustrates how assembly and translation factors cooperate to promote the formation of an interface that lacks many mature subunit contacts but is stabilized by the universally conserved Dim1. The structure also shows how this interface leads to unfolding of the platform, which allows for temporal regulation of the ATPase Fap7, thus linking 40S maturation to quality-control during ribosome assembly.

Significance Statement

80S-like ribosomes are essential intermediates in 40S ribosome maturation that couple maturation to quality control. However, the structural basis for these activities and their temporal regulation remains unknown. This work addresses this knowledge gap with a structure of 80S-like ribosomes that reveals not only new roles for assembly factors in the formation of this intermediate, but also the structural basis for the temporal regulation of its resolution via the essential ATPase Fap7.

Main Text

Introduction

Ribosome assembly involves the co-transcriptional processing and folding of rRNA, which is coupled to the binding of ribosomal proteins (RPs) via a machinery of nearly 200 assembly factors (AFs). Largely assembled precursors retaining only seven AFs (Tsr1, Dim1, Nob1, Pno1, Enp1, Ltv1, and Rio2) are exported into the cytoplasm (1, 2). There, maturation is coupled to quality control in a translation-like cycle where pre-40S ribosomes bind mature 60S subunits in an eIF5B-dependent manner to produce 80S-like ribosomes (3-5). Paradoxically, 80S-like ribosomes retain Tsr1 and Dim1 (as well as Nob1 and Pno1), even though the position of Dim1 and Tsr1 is expected to block the binding of mature 60S subunits (6). Moreover, Tsr1 blocks premature formation of translation-competent 80S-ribosomes and Dim1 blocks the binding of the translation initiation factor eIF1 (6). Thus, their dissociation must be temporally regulated to allow for translation initiation only after maturation and quality control are complete.

We have previously shown that the ATPase Fap7 releases Dim1 from 80S-like ribosomes after testing their ability to faithfully translocate mRNA. Bypass of this step allows release of defective ribosomes into the translating pool (5).

Despite their central role for quality control and maturation, the structure of 80S-like ribosomes has not been described. How they are formed, despite the presence of AFs that block subunit joining, remains unclear. Furthermore, how they enable temporal regulation of Fap7 activity is also unknown. Therefore, we used single-particle cryogenic electron microscopy (cryo-EM) to visualize the structure of 80S-like ribosomes that accumulate upon Fap7 depletion (5). The structure is validated by biochemical data herein, as well as previous structural and biochemical data, and illuminates how 80S-like ribosomes harboring Dim1 and Tsr1 form, despite their position blocking subunit joining in earlier intermediates. Furthermore, structural and biochemical data also reveal how 80S-like ribosomes enable quality control.

Results and Discussion

To better understand how 40S ribosome maturation is quality-controlled via structural and functional mimicry of translation events, we used cryo-EM to visualize the structure of 80S-like ribosomes. These ribosome assembly intermediates were accumulated by Fap7 depletion (4, 5) and purified via a TAP-tag on Tsr1 (7-9), which is fully functional **(Fig. S1a)**. SDS-PAGE, mass-spectrometry, and Western blot analysis demonstrate that these intermediates retain the AFs Tsr1, Dim1, and Pno1, but Nob1 is substoichiometric (**Fig. S1b-c)**. Additionally, 60S RPs and ribosome associated factors like the SSA/SSB chaperones were identified, consistent with the presence of 25S rRNA (5). Importantly, previous biochemical data confirmed that these intermediates are on pathway because addition of recombinant Fap7/ATP releases Dim1 (5).

Initial classification identified two populations of particles. One refined to a resolution of 3.6 Å and had features like mature 80S ribosomes (**Fig. S1d-f**), similar to a recently noted 80S pre-ribosome lacking AFs (10). This subclass lacks Tsr1, Dim1, and Pno1; its platform, beak, decoding helix, and B3 bridge are in their mature conformation; and there is no density for any tRNA (**Fig. S1g**). This subclass is not described further as its significance is unclear.

The other subclass had strong 60S, but weaker pre-40S, density (**Fig. S1d-f**). Further refinement improved the clarity of the pre-40S and 60S to overall resolutions of 3.7 Å and 3.4 Å, respectively (**Fig. S1h**). Although the particles showed no preferred orientation, the resolution of pre-40S

remained anisotropic (**Fig. S1i-l)**. Local classification described below clarified the interface and platform to ~5.5-8.5 Å-resolution (**Fig. S1m-n**).

Pre-40S movements

Multi-body analysis (11) showed three main motions (**Fig. S2a**), where pre-40S rotates out from 60S and parallel to the interface (**Fig. S2b**), freed by fewer subunit bridges (**Fig. S3**). The first Eigen vector describes motions that resemble extreme translocation movements, consistent with the role of 80S-like ribosomes in quality control of the ability to carry out these movements. Notably, the position of pre-40S relative to 60S is consistent with solution footprinting, which showed that 80S-like ribosomes are in a state resembling the post-translocation "classic" state (12). In fact, 80S-like ribosomes appear hyper-classic in the composite assembly, 23° from the rotated state (**Fig. S4**). In contrast to mature 40S where the head moves independently (11), pre-40S moves as a rigid body, perhaps because Tsr1 holds together the body and head. Additionally, or alternatively, the neck, which is the point of head movement, has not yet formed.

Immature subunit interface

Previous structural analyses demonstrated that Dim1 and Tsr1 inhibit subunit joining. Dim1 sterically blocks 60S binding (6, 10, 13, 14). Tsr1 blocks eIF5B and stabilizes a conformation of h44 that perturbs its subunit bridges and leads it to clash with 60S (6, 10, 13, 14). To accommodate these AFs and h44, pre-40S is opened away from 60S, creating space between the subunits to allow movement of Tsr1 and Dim1 relative to their position in isolated pre-40S (**Fig. 1a-c**). Consequently, the 80S-like subunit interface is formed by fewer bridges than in mature 80S. For example, the B1a/b/c bridges, which involve the 40S head, are not yet formed because the pre-40S head is far from the 60S central protuberance (**Fig. 1c and S3**). Similarly, pre-40S turns away from 60S on the platform side and towards it on the beak side, thus bridge B7a cannot form because that side of the head is too distant from 60S. Further, the twisted position of pre-40S relative to 60S accommodates the immature position of h44, which is shifted left, preventing formation of the B3 and B5 bridges at the top of h44 (10, 13). In contrast, eukaryote-specific bridges at the 40S foot are largely maintained. In the case of a B5/B8-like bridge between h44 and Rpl23/uL14 and a B6-like bridge between h44 and Rpl24, the inter-subunit connections shift due to the novel orientations of the subunits but involve analogous interactions between similar structural elements (**Fig. S5**).

A striking difference between 80S-like and mature 80S ribosomes is the interaction between H69 and the small subunit. In mature ribosomes, H69 binds h44 (15) to establish the B2a bridge. This bridge is the target of RRF (16), which dissociates ribosomes, as well as some antibiotics (17-19), supporting its importance. In 80S-like ribosomes, H69 binds h24 (**Fig. 1d-e**), which moves substantially from its mature position. Although the moderate resolution of the subunit interface prevents us from modeling atomic interactions between H69 and h24, two helical densities can be assigned to H69 and h24 with high confidence. The local resolution of one helix is ~5.5 Å, lower than 60S but sufficiently well-resolved to model H69 in its mature position (**Fig. 1e and S1m**). The tip of the other helix is resolved at ~8.5 Å; however, it connects to the well-resolved base of a repositioned h24, strongly suggesting that the RNA that binds H69 derives from h24 (**Fig. 1e and S1m**). We validated interactions between Dim1 and h24, as well as Dim1 and 60S, in biochemical experiments described below.

Dim1 stabilizes h24 and binds 60S

In pre-40S, Dim1 sterically blocks approach of H69 from 60S, inhibiting subunit joining (6, 10, 13, 14). This conflict is not resolved by the remodeled interface, because H69 remains the main connection between the subunits. Instead, the map shows that Dim1 repositions with h24, moving above H69 to alleviate the steric conflict (**Fig. 2a-b and Movie S1**). This movement essentially releases Dim1 from pre-40S, maintaining contact with h24 while promoting its interaction with 60S, thus priming Dim1 for release.

To validate the position of Dim1 (despite local classification, it is resolved at ~8.5 Å) and probe the importance of contacts between Dim1 and h24, as well as Dim1 and 60S, we created Dim1 variants and tested their effects on subunit joining. In 80S-like ribosomes residues altered in Dim1-FRK (F231L/R233E/K234E) face h24 (**Fig. 2b**), while residues altered in Dim1-IKN (I250A/K253A/N254A) face across the interface toward Rpl11 and the C-terminus of Rpl42 (**Fig. 2b**). Residues altered in Dim1-MKRSL (M115A/K116E/R166E/S170A/L171A) interact with both h24 and H69. None of these residues form interactions in pre-40S ribosomes (**Fig. 2c)**. To test if the altered residues are important for formation of 80S-like ribosomes, we used an *in vivo* assay. Variants were expressed in a galactose-inducible/glucose-repressible Dim1/Fap7 yeast strain, supplemented with plasmids encoding wild-type or variant Dim1 and no or inactive Fap7. In strains competent for 80S-like ribosome formation, accumulation of 80S-like ribosomes upon depletion or inactivation of Fap7 leads to co-sedimentation of pre-18S and 25S rRNA in 80S-sized fractions (4, 5). Each variant expresses and shifts the equilibrium between 40S and 80S-like ribosomes away

from 80S-like ribosomes (**Fig. 2d-h**), demonstrating a role for these residues in the formation of 80S-like ribosomes. Thus, these biochemical data validate interactions between Dim1 and both h24 and 60S, establishing a role for Dim1 in stabilizing 80S-like ribosomes.

Tsr1 promotes the opened interface

In earlier 40S assembly intermediates, Tsr1 binds between the body and head, with its N-terminal α-helix inserted behind h44 to force it away from the body, blocking formation of canonical 80S ribosomes ((6, 10, 13, 14), **Fig. S6a**). In 80S-like ribosomes, the C-terminal domain is repositioned towards the beak's tip via a rigid-body movement around a hinge at Ala63 within the N-terminal helix, which remains behind h44 (**Figs. 3a, S6b-c, and Movie S2**).

To test the importance of this hinge, we deleted the N-terminal helix (Tsr1-ΔN74) and assessed the effect on cell growth and formation of 80S-like ribosomes. In yeast strains where endogenous Tsr1 is under a galactose-inducible/glucose-repressible promoter, providing Tsr1-ΔN74 on a plasmid produces a lethal growth phenotype (**Fig. S6d).** Moreover, **Fig. 3b** shows that formation of 80S-like ribosomes *in vivo* is strongly reduced by truncating Tsr1. Thus, the hinge in Tsr1 supports the formation of 80S-like ribosomes.

While eIF5B is required for formation of 80S-like ribosomes (3, 4), its binding is incompatible with the position of Tsr1 in previously described earlier pre-40S intermediates (20). To visualize if Tsr1 repositioning enables eIF5B binding, we superimposed 60S from the mature 80S•eIF5B complex onto this intermediate to place eIF5B ((21) **Figs. 3c-d and S6e-f**). This analysis suggests that the postulated clashes between Tsr1 and eIF5B (20) are largely resolved in 80S-like ribosomes. Notably, it is the opened subunit interface that provides space for concurrent binding of eIF5B and Tsr1 at the subunit interface, not Tsr1 repositioning.

In our previous dataset of earlier 40S assembly intermediates (14), Tsr1 is similarly rotated in a small population of molecules (**Fig. S7a**). In this low-resolution structure, Tsr1 has a disordered C-terminal domain due to its mobility in isolated pre-40S and/or the low number of particles. Nonetheless, this observation suggests that its movement away from h44 to the beak is intrinsic to Tsr1.

The structure of 80S-like ribosomes clarifies multiple roles for Tsr1 in the formation of 80S-like ribosomes versus canonical 80S ribosomes: (i) Tsr1 forces out h44, thereby sterically preventing the subunits from close approach to form the canonical subunit bridges in the head (**Figs. 1a and**

S6b); (ii) Tsr1 stabilizes the interface due to its interaction with both pre-40S and 60S (**Fig. S7b)**; (iii) Tsr1 blocks access of eIF5B to its typical binding site on 40S, instead enforcing a position where eIF5B blocks formation of the strong and early-forming B3 bridge (22) (**Fig. 3c-d**). Thus, the structure suggests that by modulating the position of eIF5B on the pre-40S Tsr1 steers the subunits away from the canonical B3-containing interface into 80S-like ribosomes.

Head folding in nascent pre-40S

Previous structures show that earlier pre-40S lack Rps10/eS10, Rps26/eS26, and Asc1 (6, 10, 13, 14), and that the tip of h31 remains unfolded (10, 13). In 80S-like intermediates, Asc1 and Rps10 locate to their mature position (**Fig. S8**), indicating these proteins are recruited prior to Fap7 activity, as expected from biochemical analyses (4). Furthermore, the tip of h31 is visible (**Fig. S9**). In earlier pre-40S intermediates, Tsr1 binds adjacent to the last ordered nucleotide in h31, and Rio2 binds adjacent to the h31's mature location (6, 10, 13, 14). Thus, we suggest that h31 folding arises from dissociation of Rio2 and detachment of Tsr1 from the head. This coincides with the beak moving to its mature position while the head straightens (**Fig. S10**).

Platform unfolding

Extensive differences between earlier pre-40S subunits and 80S-like ribosomes are observed at the platform, which is opened towards 60S via a rigid body motion (**Fig. 1c**). This movement is presumably facilitated by repositioning of h24 from the platform to the subunit interface, accompanied by disorder in the tip of h23 and partial loss of Rps1 and Rps14, as previously observed (4), requiring local classification to improve its resolution. The other 80S ribosome subclass we observe has a canonical platform (**Fig. S1g**), ruling out artifacts during sample preparation as causative for the rearrangements. Further, the particles do not adopt a preferred orientation in the ice (**Fig. S1i**), as expected if they were interacting with the air-water interface to unfold the platform. We therefore conclude that these changes represent folding transitions during 40S subunit maturation.

To interpret the platform structure, we placed Rps1•Rps14•Pno1 from the earlier pre-40S intermediates in the platform density with rigid body fitting, assuming the Rps14•Pno1 dimer remains unaltered (**Fig. 4a**). To validate this assumption, we produced mutants in the Rps14•Pno1 interface, Rps14-R107E and Pno1-QDF (Q153E/D157R/F237A, **Fig. 4b**). These variants were tested for growth defects in galactose-inducible/glucose-repressible Rps14 and Pno1 strains,

respectively, where both demonstrated growth phenotypes (**Fig. S11a-b**). Because Pno1 and Rps14 are both bound (but do not yet interact) in early 90S precursors (23-25), we used Northern analysis to confirm that these mutations do not substantially affect early maturation events. Pno1 or Rps14 depletion reduce 20S rRNA >20-100 fold, respectively (23-25, **Fig. S11c-d**). In contrast, 20S rRNA levels are reduced ~ 2-fold in the Rps14-R107E and Pno1-QDF mutants, and accumulation of 23S rRNA is not observed. Thus, lethal or near-lethal growth defects from these mutants do not arise from early maturation defects. Next, we used sucrose-gradient fractionation to assess if Pno1 binding to 80S-like ribosomes is affected in these mutants. 80S-like ribosomes were accumulated via depletion of Fap7 (4), and Western analysis was used to probe the sedimentation of Pno1. As expected from a weakened Pno1•Rps14 interface, the fraction of free Pno1 increases in both mutants relative to their isogenic wild type controls (**Fig. 4c-d**). These data strongly suggest that the Pno1•Rps14 interface is maintained in 80S-like ribosomes, supporting placement of the unchanged Rps1•Rps14•Pno1 complex in the platform density. Note that Nob1 was not identified in the EM density, presumably due to its substoichiometric presence (**Fig. S1b-c)** and its mobility, which has precluded its visualization in earlier studies that did not employ crosslinking (6, 10, 13, 14). Similarly, density corresponding to ITS1 is not visible, as also observed in previous structures (6, 10, 13, 14).

Temporal Regulation of Fap7

The intermediates studied here were purified from Fap7-depleted cells. Consistently, addition of Fap7•ATP to these intermediates leads to Dim1 release (5). To confirm that the molecules can bind Fap7 stably, we developed a binding assay where we add either Fap7 or Fap7•Rps14 in the presence of either ATP or the non-hydrolyzable ATP-analog AMPPNP to the 80S-like ribosomes herein, and assay for binding by co-sedimentation with ribosomes. These data show that Fap7 binds these intermediates. Addition of Rps14 stabilizes binding 2-3-fold, consistent with reduced occupancy of Rps14 in the purified particles. In addition, AMPPNP stabilizes binding over ATP (**Fig. 4e),** consistent with ATPase-dependent release of Dim1 (and presumably Fap7) from 80S-like ribosomes (5). Unfortunately, we were unable to obtain a structure from these Fap7-bound ribosomes, presumably due to partial occupancy. Nonetheless, we used docking to better understand how Fap7 functions in Dim1 release. By superimposing the crystal structure of Fap7•Rps14 (26) onto Rps14, Fap7 is positioned adjacent to Dim1 (**Fig. 4f**), consistent with biochemical data that show Fap7 bridges Dim1 and Rps14 (5). Intriguingly, only one of the two

crystallized Fap7•Rps14 interfaces places Fap7 in 80S-like ribosomes – the other clashes with the platform (**Fig. S12a-b**).

To validate the position of Fap7, we created mutations in Fap7 and Rps14 that would affect this interface. Rps14-K49E and Fap7-RYD (R114E/Y116A/D118K) alter residues that contact their binding partners only in the dockable interface, whereas Rps14-RVM (R41E/V42L/M46A) alters an arginine that binds Fap7 in both (Val42 and Met46 bind Fap7 in the dockable interface) (**Figs. 4f, S12c**). Each mutation results in a substantial growth phenotype (**Fig. S12d**). Furthermore, recombinant Fap7-RYD and Rps14-RVM bind Rps14 and Fap7 more weakly (**Fig. 4g**). Finally, as in inactive Fap7 (5), the growth phenotype from Fap7-RYD is partially rescued by a self-releasing Dim1 mutation, Dim1-EKR (**Fig. 4h**). Together, these experiments support this placement of Fap7 in 80S-like ribosomes. Additionally, this biochemically-validated position of Fap7 between Rps14 and Dim1 also validates interpretation of the medium-resolution features of the map: Rps14 on the platform and Dim1 at the subunit interface.

Fap7 binds Rps14 (5, 26, 27) and the biochemical data above demonstrate the importance of their interaction for 40S maturation and Dim1 release (5). Rps14 is bound in the earliest nucleolar 40S assembly intermediates (23-25), yet Fap7-dependent Dim1 release is one of the last cytoplasmic steps in maturation, raising the question how Fap7 recruitment to nascent ribosomes is temporally regulated. Docking Fap7 onto earlier pre-40S intermediates demonstrates that it would clash with the tip of h23 within the platform (**Fig. S12b**). In contrast, in 80S-like ribosomes this steric conflict is relieved by opening of the platform, which repositions Rps14, and mobilizes h23. Thus, unfolding of the platform in 80S-like ribosomes allows for temporal regulation of Fap7 binding and activity to 80S-like ribosomes (**Fig. 4i**).

In summary, the structure of 80S-like ribosomes presented here, validated by genetic and biochemical data herein, as well as previous biochemical (5), mass spectrometry (4), and crystallographic (26) data, reveal unexpected features that allow for reconciliation and explanation of many previous observations. (i) 80S-like ribosomes display an opened interface whose formation is enabled by Tsr1. Tsr1 blocks the canonical binding mode of eIF5B, required for subunit joining; supports a conformation of the decoding helix that necessitates an open interface; and stabilizes the complex by binding both subunits. (ii) the subunit interface in 80S-like ribosomes is stabilized by an interaction between H69 from 60S with h24 from pre-40S, stabilized by Dim1. (iii) Because h24 is a component of the platform, this interaction opens the platform towards 60S and mobilizes constituent RNAs and proteins. (iv) Platform remodeling allows for temporal regulation of the

ATPase Fap7, which links dissociation of Dim1 to quality control (5). Thus, this structure explains how formation of 80S-like ribosomes is required for proofreading of 40S ribosome maturation.

Materials and Methods

Yeast strains/cloning: Yeast strains (**Table S1**) were produced using PCR-based recombination (28), and confirmed by PCR and Western blotting. Mutations in Dim1, Fap7, Tsr1, Pno1, and Rps14-expressing plasmids were introduced by site-directed mutagenesis, confirmed by sequencing.

Growth assays: Doubling times were measured in a Synergy 2 microplate reader (BioTek Instruments, Winooski, VT) as described (5). Statistical analyses were performed using Prism v.6.02 (GraphPad Software, La Jolla, CA).

Sucrose density gradient analysis: Sucrose gradient fractionations of whole cell lysates, followed by Northern and Western blot analysis, were performed as described (4). 40S and 80S fractions were quantified using Quantity One 1-D Analysis Software v.4.1.2 (Bio-Rad Laboratories, Hercules, CA). Pno1 was quantified using ImageJ Software v1.52 (100) (Rasband, W.S., ImageJ, U. S. National Institutes of Health, Bethesda, Maryland, USA, https://imagej.nih.gov/ij/, 1997-2018).

Antibodies: Antibodies against recombinant Rps10, Dim1, Nob1, Pno1, Rio2, and Tsr1 were raised in rabbits (Josman, LLC, Napa, CA). Antibodies against Rpl3 or eEF2 were gifts from J. Warner. or T. Goss-Kinzy, respectively.

Protein binding: MBP-Fap7(-RYD) and SUMO-Rps14(-RVM) were expressed and purified as described (5). Protein binding assays were performed as described (5). 3 µM MBP-Fap7/MBP-Fap7-RYD was mixed with 4.4 µM SUMO-Rps14/SUMO-Rps14-RVM in binding buffer (BB, 50 mM Tris pH 7.5/150 mM NaCl/5% glycerol), applied to amylose resin, washed, and bound proteins eluted in BB + 50 mM maltose.

Ribosome binding assay: 80S-like ribosomes were affinity-purified from Tsr1-TAP; Gal::Fap7 cells grown in YPD medium for 16 h as described (5). 20 nM 80S-like ribosomes were incubated with 70 nM purified, recombinant Fap7 or Fap7+SUMO-Rps14 complex in 50 µL of buffer (30 mM HEPES-KOH [pH 6.8], 100 mM NaCl, 6 mM $MgCl_2$, 0.5 mM EDTA, and 1 mM DTT). ATP or AMPPNP was added to a final concentration of 0.5 mM. The samples were incubated on ice for 15 min, placed on 400 µL of a 20% sucrose cushion, and centrifuged for 2 h at 400,000g in a TLA 100.1 rotor. The supernatant was removed, pellets resuspended in SDS loading dye and analyzed by western blotting.

Cryo-EM: 80S-like ribosomes from Fap7-depleted cells were affinity-purified as described (5). After elution, the concentration was determined on a Nanodrop 1000 (ThermoFisher Scientific, Waltham, MA). 3 µL of 72 nM eluate was applied to a plasma-treated UltraAuFoil grid (Quantifoil, Großlöbichau, Germany). Grids were hand blotted before freezing in liquefied ethane.

Images were acquired on a ThermoFisher/FEI Titan Krios transmission electron microscope operating at 300 kV, equipped with a DE64 camera (Direct Electron, San Diego, CA) directed by the automated hole finder in Leginon (29). Images were recorded in "movie mode" at 1.3-2.5 µm defocus. 25 $e^-/Å^2$ dose was spread over 42 frames at a nominal magnification of 59,000x, yielding

1.24 Å/pixel at the specimen level. 4,193 micrographs were frame aligned and dose compensated with MotionCorr (30). Initial CTF parameters were estimated using Gctf (31). 146,641 particles were auto-picked in Relion-3.0, with per-particle CTF estimation/correction and beam-tilt correction (32). 3D classification revealed 55,949 80S particles. 90,692 particles were 80S-like ribosomes (**Fig. S1, Tables S2-5**).

Mature and 80S-like ribosomes were independently "autorefined" in Relion3.0 to 3.6 and 3.4 Å resolution, respectively. The parent 80S-like structure revealed an anisotropic pre-40S and was further refined with a custom mask on either subunit, yielding structures of pre-40S and 60S at 3.7 and 3.4 Å-resolution, respectively (**Fig. S1**). For multi-body refinement of the parent structure in Relion-3.0 the 60S, including the H69/h24 bridge, was the first body and pre-40S was the second body with 11-Å overlapping masks (**Fig. S2**).

Local classification/refinement: Local classification was performed on a bin-2 stack using a spherical mask around H69 or the platform. For the H69 bridge, a dominant subclass (43,893 particles) was autorefined with masking on 60S to reveal the position of Dim1 at ~7.5 Å resolution (**Fig. S1b**). H69 is resolved at ~5.5 Å and contours of its major and minor grooves are visible. Finally, the repositioned h24 has a resolution of ~8.5 Å and the twist of the helix is visible. These central elements are identifiable within the resolution limits because (i) they connect to well-resolved parts of the structure; (ii) the distinct helical contours of the RNA; and (iii) the two-domain construction of Dim1.

For the platform a dominant class (36,914 particles) was autorefined with a mask on pre-40S (**Fig. S1b**). The platform density follows the contours of an unchanged Rps1•Rps14•Pno1 complex, supported by mutagenesis.

Modelling: 60S and pre-40S were modeled from 80S ribosomes (PDB 3J77, (33) using Chimera (34) to rigid body fit each subunit followed by manual adjustment in Coot (35). Rpl41, h23, h45, Rps1, Rps26, and Rps14 were removed with adjustments to Rpl19, H69, and the L1 stalk. In pre-40S, h24 was moved as a rigid body to match the contours of the remodeled bridge. Additionally, the head RNA and proteins were positioned into that density. Tsr1 from PDB 6FAI (10) was fit as a rigid body. Yeast Dim1 was modeled in SwissModel (36) and, after rigid-body fitting into the bi-lobed density, α-helices and β-sheets were manually placed, followed by refinement with "Phenix.real.space.refine" (37). The model matched the density with a correlation coefficient (CC) of 0.8. Rps1•Rps14•Pno1 was fit into the segmented platform density, matching the density with a CC of 0.6. Each model was independently refined with "Phenix.real.space.refine" (37). Pre-40S had 89.7% residues in favored Ramachandran regions and 0.2% in outlier region (13% Clashscore). 60S had 85.9% residues in favored Ramachandran regions and 0.2% in outlier region (27.9% Clashscore).

Acknowledgments
This work was supported by NIH grants R01-GM117093 and R01-GM086451, and HHMI Faculty Scholar grant 55108536 to K.K.. The authors acknowledge the use of instruments at the Biological Science Imaging Resource supported by Florida State University and NIH grants S10 RR025080, S10 OD018142, and U24 GM116788. H.G. was supported in part by a PGA National Women's Cancer Awareness Postdoctoral Fellowship. We wish to thank members of the Karbstein lab for comments on the manuscript, and Drs. Scott Stagg and Kenneth Taylor for useful discussions. Structure figures were made in Chimera and assembled in Photoshop (Adobe, San Jose, CA) without modification. Maps and coordinates have been uploaded to the PDB and EMDB (6WDR/21644, 6OIG/20077, 20071, 20072, 20211, and 20075).

References:

1. J. Baßler, E. Hurt, Eukaryotic Ribosome Assembly. *Annu Rev Biochem* **88**, 281-306 (2019).
2. S. Klinge, J. L. Woolford, Ribosome assembly coming into focus. *Nat Rev Mol Cell Biol* **20**, 116-131 (2019).
3. S. Lebaron *et al.*, Proofreading of pre-40S ribosome maturation by a translation initiation factor and 60S subunits. *Nat Struct Mol Biol* **19**, 744-753 (2012).
4. B. S. Strunk, M. N. Novak, C. L. Young, K. Karbstein, A translation-like cycle is a quality control checkpoint for maturing 40S ribosome subunits. *Cell* **150**, 111-121 (2012).
5. H. Ghalei *et al.*, The ATPase Fap7 Tests the Ability to Carry Out Translocation-like Conformational Changes and Releases Dim1 during 40S Ribosome Maturation. *Mol Cell* **68**, 1155 (2017).
6. B. S. Strunk *et al.*, Ribosome assembly factors prevent premature translation initiation by 40S assembly intermediates. *Science* **333**, 1449-1453 (2011).
7. H. Ghalei *et al.*, The ATPase Fap7 Tests the Ability to Carry Out Translocation-like Conformational Changes and Releases Dim1 during 40S Ribosome Maturation. *Molecular cell* **67**, 990-1000 e1003 (2017).
8. S. Lebaron *et al.*, Proofreading of pre-40S ribosome maturation by a translation initiation factor and 60S subunits. *Nat Struct Mol Biol* **19**, 744-753 (2012).
9. V. Mitterer *et al.*, Conformational proofreading of distant 40S ribosomal subunit maturation events by a long-range communication mechanism. *Nature communications* **10**, 2754 (2019).
10. A. Scaiola *et al.*, Structure of a eukaryotic cytoplasmic pre-40S ribosomal subunit. *EMBO J* **37** (2018).
11. T. Nakane, D. Kimanius, E. Lindahl, S. H. Scheres, Characterisation of molecular motions in cryo-EM single-particle data by multi-body refinement in RELION. *Elife* **7** (2018).
12. H. Ghalei *et al.*, Hrr25/CK1delta-directed release of Ltv1 from pre-40S ribosomes is necessary for ribosome assembly and cell growth. *J Cell Biol* **208**, 745-759 (2015).
13. A. Heuer *et al.*, Cryo-EM structure of a late pre-40S ribosomal subunit from. *Elife* **6** (2017).
14. M. C. Johnson, H. Ghalei, K. A. Doxtader, K. Karbstein, M. E. Stroupe, Structural Heterogeneity in Pre-40S Ribosomes. *Structure* **25**, 329-340 (2017).
15. A. Ben-Shem *et al.*, The structure of the eukaryotic ribosome at 3.0 Å resolution. *Science* **334**, 1524-1529 (2011).
16. R. D. Pai *et al.*, Structural Insights into ribosome recycling factor interactions with the 70S ribosome. *J Mol Biol* **376**, 1334-1347 (2008).
17. M. A. Borovinskaya *et al.*, Structural basis for aminoglycoside inhibition of bacterial ribosome recycling. *Nat Struct Mol Biol* **14**, 727-732 (2007).
18. I. Prokhorova *et al.*, Aminoglycoside interactions and impacts on the eukaryotic ribosome. *Proc Natl Acad Sci U S A* **114**, E10899-E10908 (2017).
19. L. Wang *et al.*, Allosteric control of the ribosome by small-molecule antibiotics. *Nat Struct Mol Biol* **19**, 957-963 (2012).
20. U. M. McCaughan *et al.*, Pre-40S ribosome biogenesis factor Tsr1 is an inactive structural mimic of translational GTPases. *Nat Commun* **7**, 11789 (2016).
21. I. S. Fernández *et al.*, Molecular architecture of a eukaryotic translational initiation complex. *Science* **342**, 1240585 (2013).
22. Z. Lu *et al.*, Gas-Assisted Annular Microsprayer for Sample Preparation for Time-Resolved Cryo-Electron Microscopy. *J Micromech Microeng* **24**, 115001 (2014).

23. J. Barandun *et al.*, The complete structure of the small-subunit processome. *Nat Struct Mol Biol* **24**, 944-953 (2017).
24. J. Cheng, N. Kellner, O. Berninghausen, E. Hurt, R. Beckmann, 3.2-Å-resolution structure of the 90S preribosome before A1 pre-rRNA cleavage. *Nat Struct Mol Biol* **24**, 954-964 (2017).
25. Q. Sun *et al.*, Molecular architecture of the 90S small subunit pre-ribosome. *Elife* **6** (2017).
26. J. Loc'h *et al.*, RNA mimicry by the fap7 adenylate kinase in ribosome biogenesis. *PLoS Biol* **12**, e1001860 (2014).
27. U. A. Hellmich *et al.*, ssential ribosome assembly factor Fap7 regulates a hierarchy of RNA-protein interactions during small ribosomal subunit biogenesis. *Proc Natl Acad Sci U S A* **110**, 15253-15258 (2013).
28. M. S. Longtine *et al.*, Additional modules for versatile and economical PCR-based gene deletion and modification in Saccharomyces cerevisiae. *Yeast* **14**, 953-961 (1998).
29. B. Carragher *et al.*, Leginon: an automated system for acquisition of images from vitreous ice specimens. *J Struct Biol* **132**, 33-45 (2000).
30. X. Li *et al.*, Electron counting and beam-induced motion correction enable near-atomic-resolution single-particle cryo-EM. *Nat Methods* **10**, 584-590 (2013).
31. K. Zhang, Gctf: Real-time CTF determination and correction. *J Struct Biol* **193**, 1-12 (2016).
32. J. Zivanov *et al.*, New tools for automated high-resolution cryo-EM structure determination in RELION-3. *Elife* **7** (2018).
33. E. Svidritskiy, A. F. Brilot, C. S. Koh, N. Grigorieff, A. A. Korostelev, Structures of yeast 80S ribosome-tRNA complexes in the rotated and nonrotated conformations. *Structure* **22**, 1210-1218 (2014).
34. E. F. Pettersen *et al.*, UCSF Chimera - A visualization system for exploratory research and analysis. *Journal of Computational Chemistry* **25**, 1605-1612 (2004).
35. P. Emsley, B. Lohkamp, W. G. Scott, K. Cowtan, Features and development of Coot. *Acta Crystallogr D Biol Crystallogr* **66**, 486-501 (2010).
36. A. Waterhouse *et al.*, SWISS-MODEL: homology modelling of protein structures and complexes. *Nucleic Acids Res* **46**, W296-W303 (2018).
37. P. D. Adams *et al.*, PHENIX: a comprehensive Python-based system for macromolecular structure solution. *Acta Crystallogr D Biol Crystallogr* **66**, 213-221 (2010).

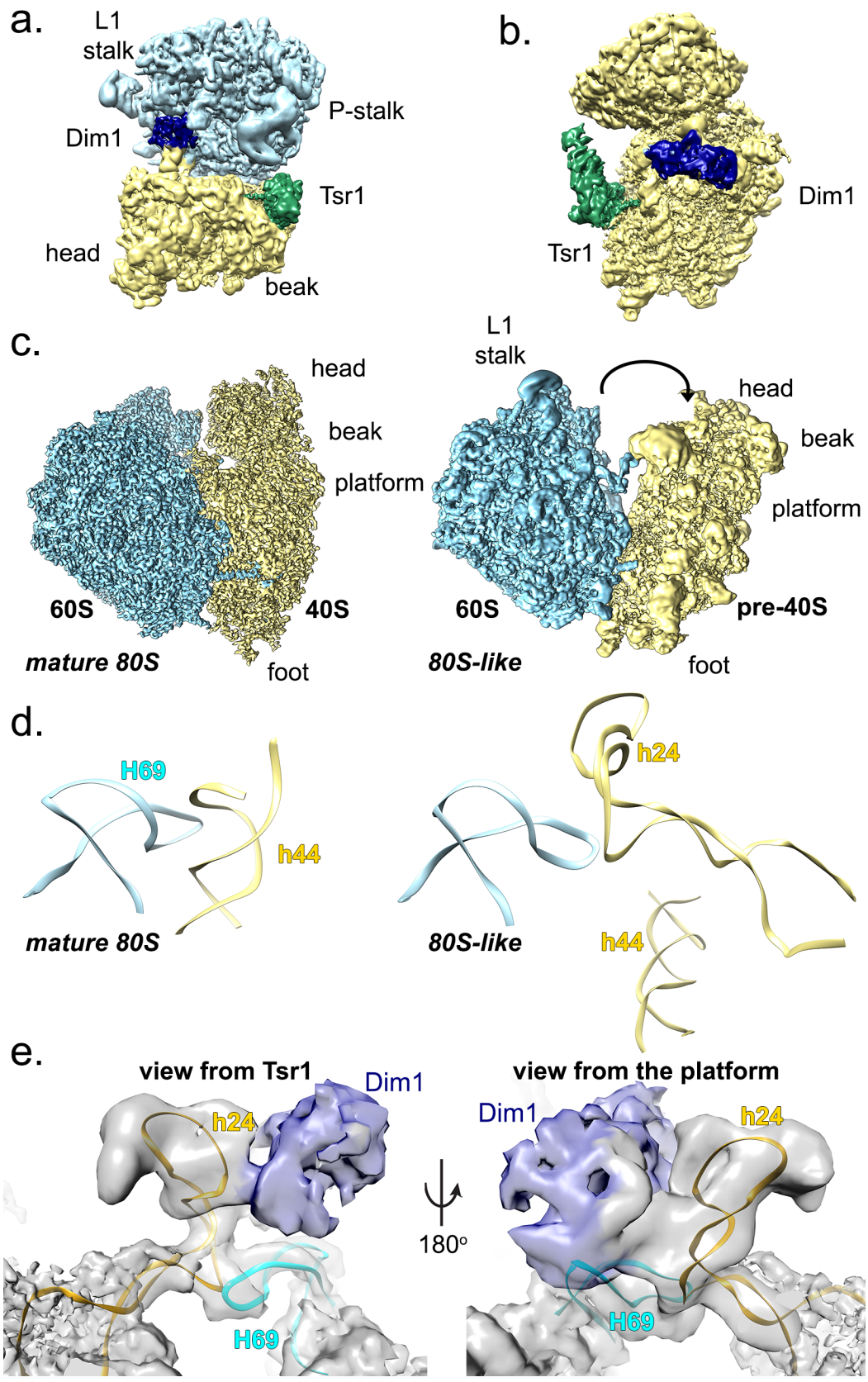

Fig. 1: 80S-like ribosomes join via an immature interface. a. Overall structure of 80S-like ribosomes. 60S is light blue, pre-40S is yellow, Dim1 is dark blue, and Tsr1 is green. **b.** The pre-40S interface has only Tsr1 (green) and Dim1 (blue) bound. **c.** In 80S-like pre-ribosomes the space between the subunits is expanded. Mature 80S/80S-like identifies each structure (bold italics). 60S/40S/pre-40S identify each subunit (bold). Structural elements are identified in each subunit (lower case). **d.** In mature ribosomes, helix 69 from the 60S subunit (H69, blue) binds helix 44 from the pre-40S subunit (h44, yellow, model from PDB ID 3J77 (33)). 80S-like ribosomes join through a novel bridge B2a/c where H69 (blue) joins a repositioned h24 (yellow). **e.** H69 and h24 fit into the density at the subunit interface.

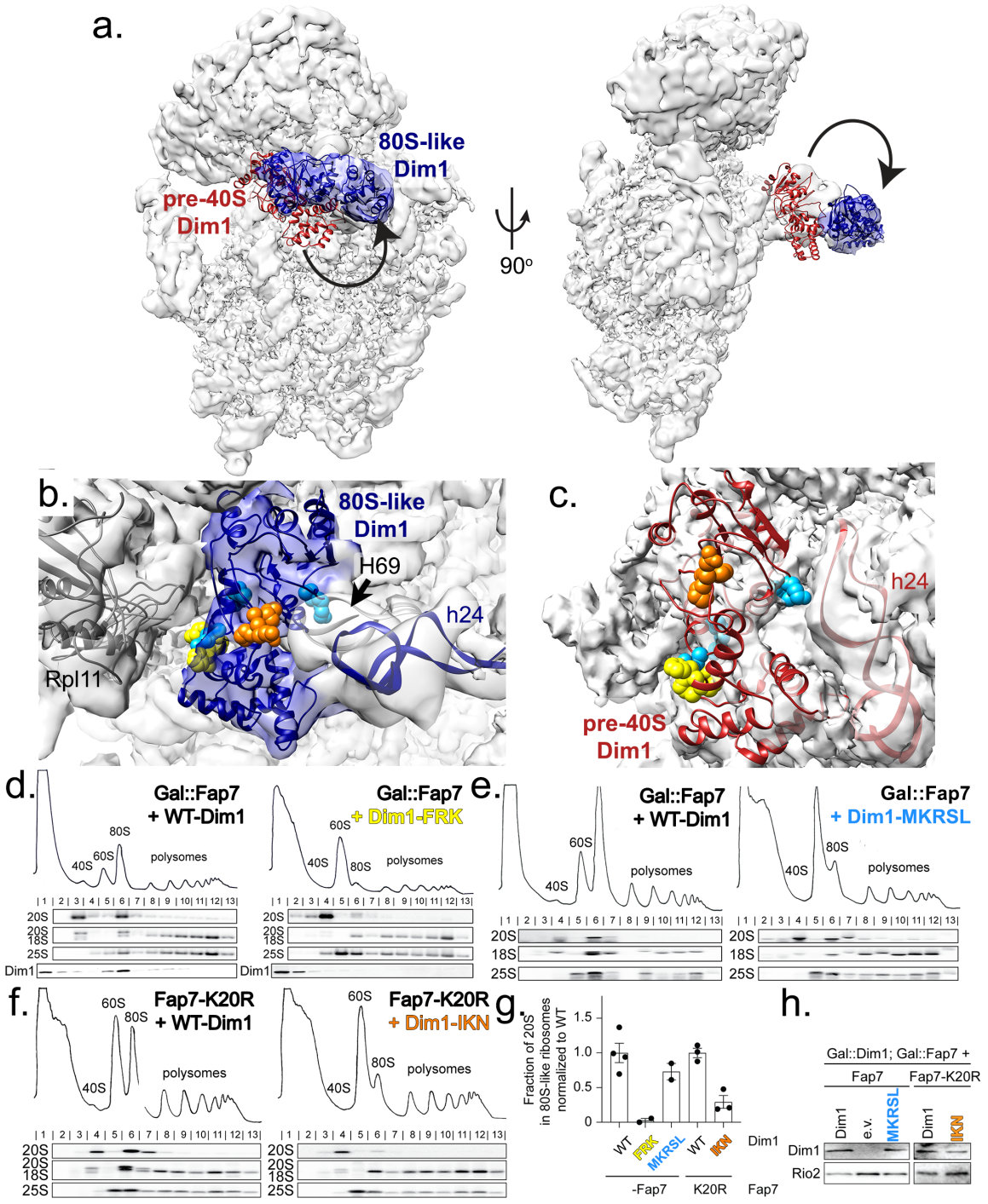

Fig. 2: Dim1 stabilizes h24 at the 80S-like pre-ribosome interface. a. Local classification followed by refinement and local B-factor sharpening in Relion 3.0 revealed a bi-lobed density at the 60S-pre-40S interface that matches the Dim1 structure (blue). The position of Dim1 in an earlier cytoplasmic pre-40S intermediate (red, Dim1 fit into EMD-4218 (13)) is also shown, demonstrating its repositioning at the interface. **b.** The Dim1-FRK residues (orange) face h24, Dim1-IKN faces Rpl11 and Dim1-MKRSL (cyan) faces h24 and H69. **c.** Neither residue makes contacts in pre-40S

subunits. **d., e., f.** Dim1-FRK, Dim1-MKRSL, and Dim1-IKN impair subunit joining. Whole cell extracts depleted of endogenous Dim1 and Fap7 (Gal::Dim1;Gal::Fap7) for 16-20 h and supplemented with plasmids encoding wild type or mutant Dim1 and no (**d., e.**) or inactive Fap7-K20R (**f.**) were fractionated on 10-50% sucrose gradients and the sedimentation of pre-40S ribosomes containing 20S rRNA was probed by Northern blot analysis and Dim1 was probed by Western blot. 80S-like ribosomes sediment in fractions 6-7 and contain 20S and 25S rRNA, while pre-40S sediment in fractions 3-5 (4, 5, 12). **g.** Quantification of the gradient Northern blots in (**d.-f.**). Fraction of 20S in 80S-like ribosomes (fractions 6-7) compared with total 20S was calculated. Data were normalized to wild type Dim1. 2 or 3 biological replicates were obtained for Dim1-FRK, Dim1-MKRSL and Dim1-IKN, respectively. Error bars indicate the standard error of the mean (SEM). **h.** Western blot of total cellular protein showed that both Dim1-MKRSL and Dim1-IKN are expressed to a similar extent as Dim1.

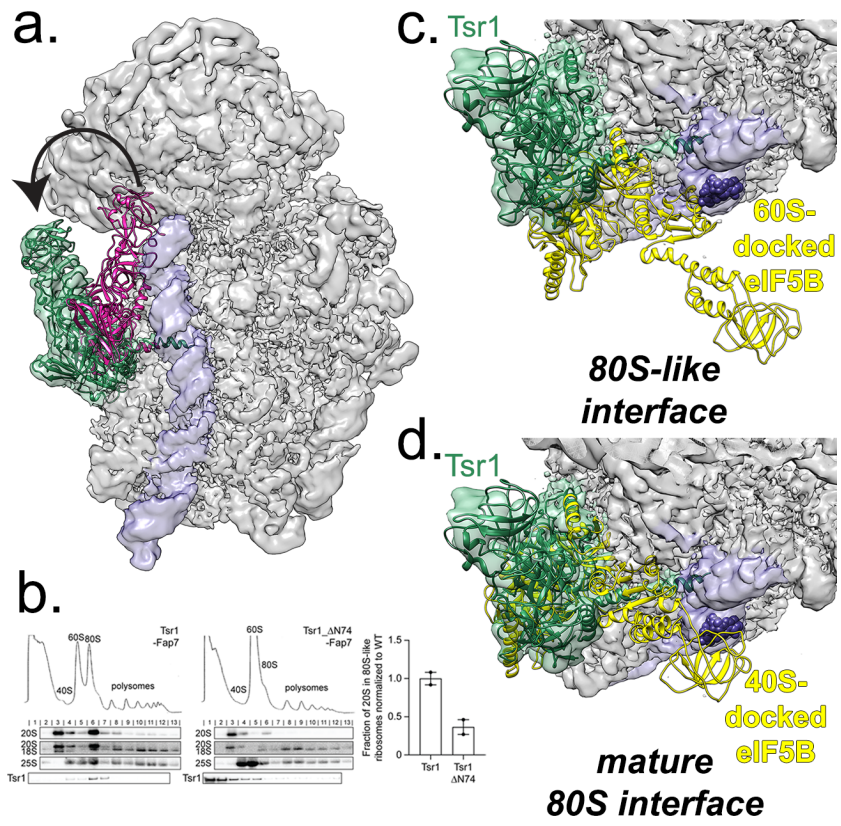

Fig. 3 Tsr1 is repositioned to the beak. a. The position of Tsr1 in 80S-like ribosomes (green) differs from the position in an earlier cytoplasmic pre-40S intermediate (pink). h44 is shown in purple (from EMD-8349 (14)). **b.** Whole cell extracts were fractionated as in Figure 2 (left). Quantification of the gradient Northern blots (right). Fraction of 20S in 80S-like ribosomes (fractions 6-7) compared with total 20S was calculated. Data are the average of two biological replicates, normalized to wild type Dim1, and error bars indicate the SEM. **c.** The opened pre-40S and 60S interface leaves space for eIF5B (yellow) across h44 (purple), blocking the early-forming B3 bridge (marked by nucleotides 1655-1657, shown as purple spheres). Model was obtained by superimposition of the 60S subunits from 80S-like pre-ribosomes and the eIF5B-bound mature 80S ribosome (PDB ID 4V8Z (21)). **d.** If subunits were joining in the canonical mature 80S-structure, Tsr1 binding would block eIF5B recruitment. Model was obtained by superimposition of the 40S subunits from 80S-like pre-ribosomes and the eIF5B-bound mature 80S ribosome (PDB ID 4V8Z (21)). The clashscore, defined in Phenix (37) as the number of overlaps greater than 0.4 Å/1000 atoms, increases from 170 (60S superimposition) to 780 (40S superimposition), an increase from 2% to 11% of the atoms in Tsr1.

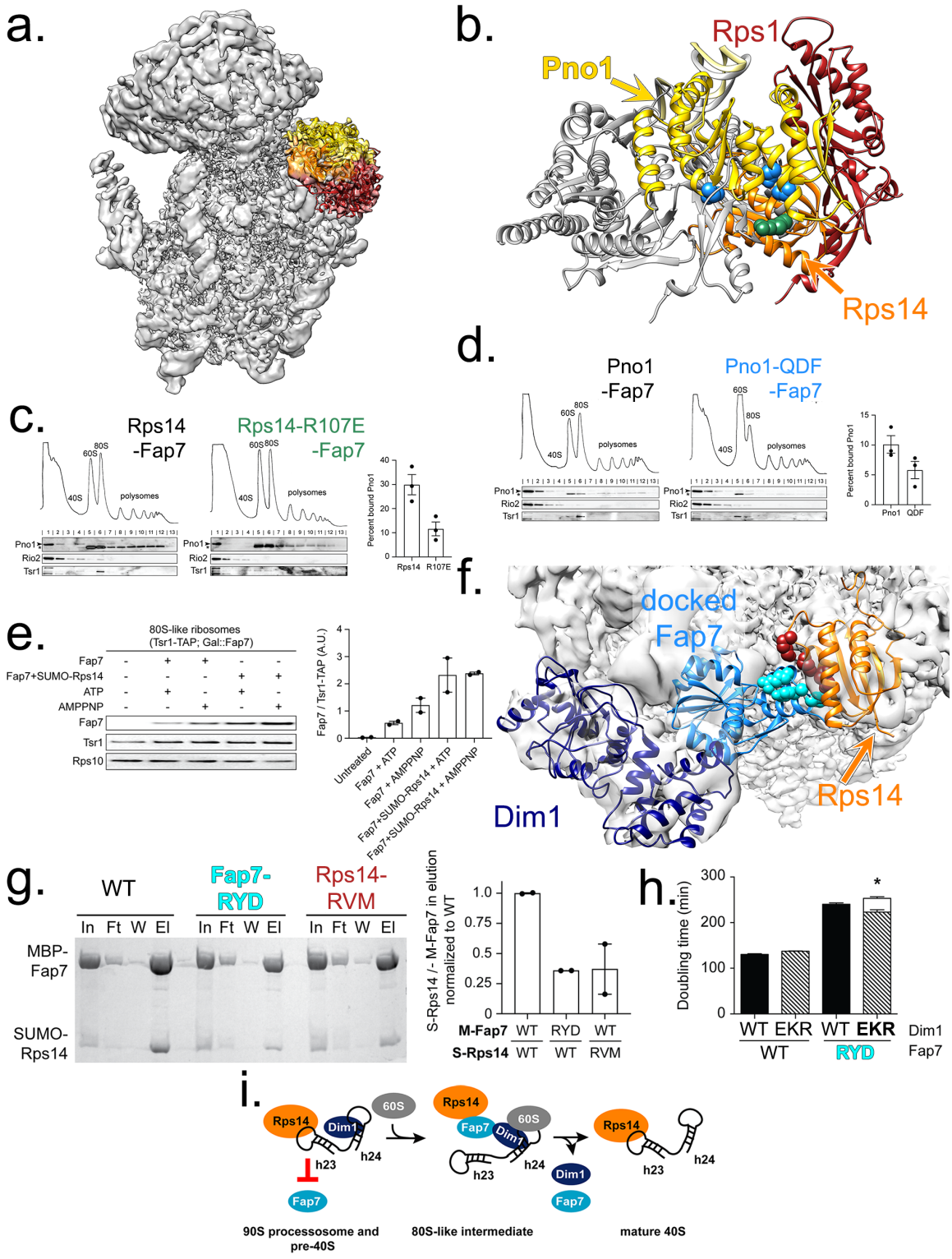

Fig. 4: An opened pre-40S platform enables temporal regulation of Fap7. a. After local classification at the platform, alignment, and local B-factor sharpening in Relion-3.0, the dominant class has density corresponding to Rps1 (red), Rps14 (orange), and Pno1 (yellow) albeit not at their final positions. **b.** In 80S-like ribosomes Rps1 (red), Rps14 (orange) and Pno1 (yellow) are shifted outwards relative to their positions in an earlier pre-40S intermediate (PDB ID 6FAI (10), Rps1, Rps14, and Pno1 in gray). The residues in Pno1-QDF (blue) and Rps14-R107 (green) are at the interface between Pno1 and Rps14. **c.** The indicated whole cell extracts were fractionated as in Figure 2 and analyzed by Western blot (left). Bound Pno1 was calculated as the percent of Pno1 in fractions 4-13 compared to total Pno1 (right). Data are the average of three biological replicates and error bars indicate SEM. Note that the top band is Pno1, while the bottom band, marked with an asterisk, represents cross-reactivity. **d.** The indicated whole cell extracts were fractionated as in Figure 2 and analyzed by Western blot (left). Bound Pno1 was calculated as in **c** (right). Data are the average of three biological replicates and error bars indicate SEM. **e.** Fap7 binds to purified 80S-like ribosomes. Fap7 binding in the presence and absence of Rps14 and ATP or AMPPNP was assessed in a pelleting assay. Ribosome pellets were probed for Fap7, Tsr1-TAP or Rps10 (left), and bound Fap7 quantified relative to the amount of 80S-like ribosomes (Tsr1-TAP, right). Data are the average of 2 replicates and error bars indicate SEM. **f.** Docking Fap7•Rps14 (Fap7, chain G and Rps14, chain F) from PDB ID 4CW7 (26) onto Rps14 (orange) in 80S-like ribosomes places Fap7 (cyan) in direct contact with Dim1 (blue), as predicted by previous biochemical data (5). The residues in Fap7-RYD (orange) and Rps14-RVM (blue) are at the interface between Fap7 and Rps14 (formed between chains G and F). **g.** Interface mutations in Fap7 or Rps14 weaken their binding affinity for each other. Shown are Coomassie-stained SDS-PAGE gels of protein binding assays on amylose beads of purified, recombinant MBP-Fap7 or MBP-Fap7-RYD and SUMO-Rps14 or SUMO-Rps14-RVM. In, input; Ft, flow-through; W, final wash; El, elution (left). Quantification of SUMO-Rps14 (S-Rps14) compared to MBP-Fap7 (M-Fap7) in elution normalized to wild type (right). Data are the average of two replicates and error bars indicate SEM. **h.** Doubling time, in minutes, of cells depleted of endogenous Dim1 and Fap7 (Gal::Dim1; Gal::Fap7) and transformed with plasmids encoding Dim1 or Dim1-EKR and either Fap7 or Fap7-RYD. The white column represents the expected doubling time if there was no rescue of Fap7-RYD by Dim1-EKR (See also (5)). The height of this column was calculated by multiplying the observed fold differences for each single mutation. The data are the average of 16-17 biological replicates and the error bars represent SEM. Unpaired t-test was performed comparing expected and actual doubling times of cells expressing Fap7-RYD and Dim1-EKR. *p-value = 0.030. **i**. The Fap7 binding site on Rps14 is blocked by h23 in nucleolar 90S pre-ribosomes (23-25) and earlier 40S assembly intermediates (10, 13). Opening of the platform temporarily removes h23, enabling Fap7 recruitment to promote Dim1 release (5).